

Photoelectron momentum distributions of triatomic CO_2 molecules by circularly polarized attosecond pulses

Si-Qi Zhang(张思琪), Jun Zhang(张军), Xin-Yu Hao(郝欣宇), Jing Guo(郭静), Aihua Liu(刘爱华), and Xue-Shen Liu(刘学深)

Citation: Chin. Phys. B, 2024, 33 (**10**): 103301. DOI: 10.1088/1674-1056/ad6b81
Journal homepage: http://cpb.iphy.ac.cn; http://iopscience.iop.org/cpb

What follows is a list of articles you may be interested in

Electron vortices generation of photoelectron of H_2^+ by counter-rotating circularly polarized attosecond pulses

Haojing Yang(杨浩婧), Xiaoyu Liu(刘晓煜), Fengzheng Zhu(朱风筝), Liguang Jiao(焦利光), and Aihua Liu(刘爱华)
Chin. Phys. B, 2024, 33 (**1**): 013303. DOI: 10.1088/1674-1056/ad011a

Dynamics of molecular alignment steered by a few-cycle terahertz laser pulse

Qi-Yuan Cheng(程起元), Yu-Zhi Song(宋玉志), Deng-Wang Li(李登旺), Zhi-Ping Liu(刘治平), and Qing-Tian Meng(孟庆田)
Chin. Phys. B, 2022, 31 (**10**): 103301. DOI: 10.1088/1674-1056/ac6eeb

Direct Coulomb explosion of N_2O^{2+} induced by monochromatic extreme ultraviolet photons at 38.5 eV

Min Zhang(张敏), B Najjari, Bang Hai(海帮), Dong-Mei Zhao(赵冬梅), Jian-Ting Lei(雷建廷), Da-Pu Dong(董达谱), Shao-Feng Zhang(张少锋), Xin-Wen Ma(马新文)
Chin. Phys. B, 2020, 29 (**6**): 063302. DOI: 10.1088/1674-1056/ab8629

Field-free molecular orientation steered by combination of super-Gaussian and THz half-cycle laser pulses

Qi-Yuan Cheng(程起元), Yu-Zhi Song(宋玉志), Qing-Tian Meng(孟庆田)
Chin. Phys. B, 2019, 28 (**11**): 113301. DOI: 10.1088/1674-1056/ab4cdf

Influence factor analysis of field-free molecular orientation

Jing-Song Liu(刘劲松), Qi-Yuan Cheng(程起元), Da-Guang Yue(岳大光), Xu-Cong Zhou(周旭聪), Qing-Tian Meng(孟庆田)
Chin. Phys. B, 2018, 27 (**3**): 033301. DOI: 10.1088/1674-1056/27/3/033301

Photoelectron momentum distributions of triatomic CO_2 molecules by circularly polarized attosecond pulses

Si-Qi Zhang(张思琪)[1,2], Jun Zhang(张军)[1], Xin-Yu Hao(郝欣宇)[1], Jing Guo(郭静)[1,†], Aihua Liu(刘爱华)[1,‡], and Xue-Shen Liu(刘学深)[1,§]

[1] *Institute of Atomic and Molecular Physics, Jilin University, Changchun* 130012, *China*
[2] *School of Physics, Harbin Institute of Technology, Harbin* 150001, *China*

(Received 18 April 2024; revised manuscript received 16 July 2024; accepted manuscript online 6 August 2024)

Molecular-frame photoelectron momentum distributions (MF-PMDs) have been studied for imaging molecular structures. We investigate the MF-PMDs of CO_2 molecules exposed to circularly polarized (CP) attosecond laser pulses by solving the time-dependent Schrödinger equations based on the single-active-electron approximation frames. Results show that high-frequency photons lead to photoelectron diffraction patterns, indicating molecular orbitals. These diffraction patterns can be illustrated by the ultrafast photoionization models. However, for the driving pulses with 30 nm, a deviation between MF-PMDs and theoretically predicted results of the ultrafast photoionization models is produced because the Coulomb effect strongly influences the molecular photoionization. Meanwhile, the MF-PMDs rotate in the same direction as the helicity of driving laser pulses. Our results also demonstrate that the MF-PMDs in a CP laser pulse are the superposition of those in the parallel and perpendicular linearly polarized cases. The simulations efficiently visualize molecular orbital geometries and structures by ultrafast photoelectron imaging. Furthermore, we determine the contribution of HOMO and HOMO-1 orbitals to ionization by varying the relative phase and the ratio of these two orbitals.

Keywords: molecular-frame photoelectron momentum distributions, single-active-electron approximation frames, ultrafast photoionization models

PACS: 33.80.–b, 42.65.Re, 33.20.Xx **DOI:** 10.1088/1674-1056/ad6b81

1. Introduction

Following rapid advances of ultrashort intense laser technology, it has become possible to image and manipulate nuclear and electronic dynamics of molecules in attosecond temporal and sub-Ångström spatial resolutions.[1–4] Free-electron laser as a new light source can provide such ultrashort time resolution and high-brightness laser pulses.[5–7] Küpper *et al.* have experimentally achieved the detection for x-ray diffraction patterns of gas targets utilizing the x-ray free-electron laser.[8] In Ref. [9] the authors reported that molecular two-photon double ionization of D_2 can be traced by using the extreme ultraviolet (XUV) free-electron laser.

Molecular-frame photoelectron momentum distributions (MF-PMDs) encode structural and dynamical information of a target system, which allows it to be used for controlling ultrafast electronic dynamics and imaging the molecular orbital.[10–14] Considerable efforts have been devoted to investigate the photoelectron momentum distributions (PMDs) of atoms and molecules based on electron diffraction and interference.[15–22] Zuo *et al.* theoretically proposed that one can extract the molecular structure from laser-induced electron diffraction (LIED) based on a pump-probe scheme.[16] LIED has been experimentally observed in O_2 and N_2, which carried the information about the molecular orbital and nuclei.[17] In Ref. [18] the authors reported that the extraction of interatomic distances of N_2 and CO_2 molecules can be realized relying on LIED. Yuan *et al.* found that ultrafast electron diffraction depends on the orbital symmetry and molecular internuclear distance.[19] Vortex patterns arising from interfering wave packets in PMDs have been observed from potassium atom exposed to a pair of circularly polarized (CP) pulses in experiment, and determining the relative phases of interfering wave packets allows one to directly measure the wave function.[23,24] Electron vortex is sensitive to the parameters of the driving attosecond pulses, such as the time delay, the carrier envelope phase and amplitude ratio of driving pulses.[25] Thus, it is possible to characterize the attosecond pulses with electron vortex.[26] It has been reported that the spider-like interference pattern in PMDs provides access to reconstruct the photoelectric ionization time on the attosecond time scale.[27]

Two-center interference effect has been shown to play an important role in many processes of strong field physics.[28–34] For instance, Lein *et al.* found that such interference leads to a pronounced minimum in harmonic spectra, and the harmonics around minimum with large ellipticity.[28,29] By analyzing the photoelectron angular distributions based on two-center interference, one can contain the relative phase shift of the emitted electron.[32] The experimental results in Ref. [33]

†Corresponding author. E-mail: gjing@jlu.edu.cn
‡Corresponding author. E-mail: aihualiu@jlu.edu.cn
§Corresponding author. E-mail: liuxs@jlu.edu.cn

© 2024 Chinese Physical Society and IOP Publishing Ltd

show that the PMDs of argon dimers are different from those of argon atoms, due to the two-center interference. The deviation between PMDs of the dimers and the basic two-center interference provides an ideal tool to study electron dynamics of dimers. In Ref. [34] the authors provided experimental evidence that two-center photoelectron interference pattern can be observed from neon dimer, this interference pattern allows for obtaining the information about the orbital parity, orbital phase and bond length. Recent studies have suggested that two-source double-slit interference effect will occur when the ionized electrons and molecular ions undergo rescattering.[35,36] Okunishi *et al.*[35] presented the differences between the high-order above-threshold ionization (HATI) spectra related to two-source double-slit interference effect of N_2 and O_2 molecules. It was indicated that HATI spectra may be used for analysis of molecular properties and inferring symmetry of the highest occupied molecular orbital (HOMO).

CO_2 is an important gas in interstellar, ionization of CO_2 is therefore a basic photochemistry process worth studying.[37] Here, we use the triatomic CO_2 molecule as a benchmark system. To accurately describe electron dynamics in ultrafast laser fields, one requires to numerically solve the time-dependent Schrödinger equation (TDSE). Recent studies have shown that the TDSE based on the single-active-electron approximation (SAE) frames is valid in simulating ultrafast dynamical processes of multi-electron molecules in mid-infrared and static laser fields.[18,38,39] In this work, we extend the SAE frames for studying molecular photonionization in x-ray/XUV high-frequency regions, and the ultrafast photoionization models[16] are adopted to describe these results. Such high-frequency photons allow neglecting additional excitation and ionization resulted from the additional excited states. Thus, we only focus on the single-photon ionization process. In addition, this study focuses on the attosecond time-resolved electron dynamics, the picosecond and femtosecond time-resolved rotational and vibrational effects of the nuclei can be ignored because these effects are much slower than the attosecond time-resolved electron dynamics.

2. Numerical methods

We perform numerical simulations on CO_2 molecules within SAE frames,[18,38] and the corresponding TDSE for a molecule aligned along the x axis can be expressed as

$$\mathrm{i}\frac{\partial\psi(\boldsymbol{r},t)}{\partial t}=\left[\frac{\boldsymbol{p}^2}{2}+V(\boldsymbol{r})+V_L(\boldsymbol{r},t)\right]\psi(\boldsymbol{r},t), \tag{1}$$

where $\boldsymbol{p}$ is the momentum of the active electron, $V(\boldsymbol{r})$ is the molecular soft-core Coulomb potential[18,38]

$$V(\boldsymbol{r})=\sum_{j=1}^{3}\frac{-Z_j(\boldsymbol{r})}{\sqrt{(\boldsymbol{r}-\boldsymbol{\rho}_j)^2+a_j^2}}. \tag{2}$$

Here, j labels three nuclei at fixed positions $\boldsymbol{\rho}_j$. $Z_j(\boldsymbol{r})=Z_j^{\infty}+(Z_j^0-Z_j^{\infty})\exp(-\boldsymbol{r}_j^2/\sigma_j^2)$ is the $\boldsymbol{r}$-dependent screened effective charge. The above parameters are the same as those in Ref. [18]. The soft-core parameter is set as $a_j=0.885$ a.u. (atomic units) to give the correct ionization energy of CO_2.

We use the imaginary-time propagation method to obtain the initial wavefunction of HOMO and the second highest occupied molecular orbital (HOMO-1), and the corresponding orbital wave functions are shown in Fig. 1. One can see that the HOMO orbital has four nodes located in four quadrants in the (x, y) plane with the π_g symmetry, whereas HOMO-1 orbital has six nodes located along the x-axis with the π_u symmetry, which are consistent with those in Ref. [18]. The C–O bond length is 2.24 a.u.,[40] the ionization energy is 13.8 eV,[18] and same as the experimental measurement reported in NIST.[41]

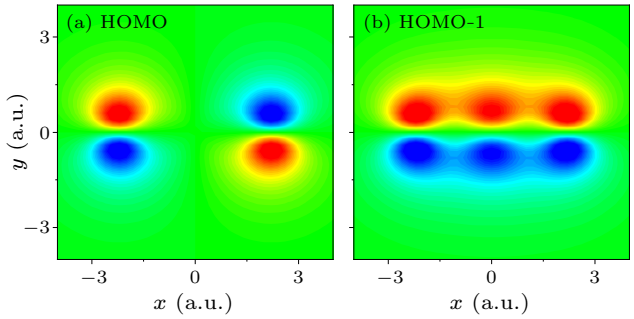


Fig. 1. Wave functions of (a) HOMO and (b) HOMO-1 for the CO_2 molecule.

The field-molecule interaction in the length gauge is $V_L(\boldsymbol{r},t)=\boldsymbol{r}\cdot\boldsymbol{E}(t)$, a CP laser field $\boldsymbol{E}(t)$ is used with the form of

$$\boldsymbol{E}(t)=E_x(t)\hat{e}_x+E_y(t)\hat{e}_y=Ef(t)[\cos(\omega t)\hat{e}_x+\sin(\omega t)\hat{e}_y], \tag{3}$$

where E and ω are the amplitude and central frequency of the driving field, and $\hat{e}_{x/y}$ is the field polarization direction. The pulse envelope is $f(t)=\sin^2(\pi t/T)$, with T being the pulse duration. For 5 nm ($\omega_0=9.11$ a.u.) the duration is $T=T_0=60\tau_0$, with one optical cycle (o.c.) $\tau_0=2\pi/\omega_0$, and $E_0=1.07$ a.u. ($I_0=4\times10^{16}$ W/cm^2). For 30 nm ($\omega_1=1.52$ a.u.), $E_1=5.34\times10^{-2}$ a.u. ($I_1=1\times10^{14}$ W/cm^2), and the duration is $T=T_1=10\tau_1$ ($\tau_1=2\pi/\omega_1$).

We use the second order split-operator method combined with fast Fourier transform (FFT) technique to solve the 2D TDSE,[42] the spatial length is taken to be 204.8 a.u., the time interval ($\Delta t=0.05$ a.u.) and the spatial step ($\Delta x=\Delta y=0.2$ a.u.) are set to ensure convergence in our calculation. To avoid spurious reflection, a $\cos^{1/8}$ absorber function is used in the absorption domain (75 a.u. $\leq|x,y|\leq$ 102.4 a.u.), which has the form of

$$g(\boldsymbol{r})=\begin{cases}1, & r\leq r_{\mathrm{b}},\\ \exp[-\beta(\boldsymbol{r}-\boldsymbol{r}_{\mathrm{b}})], & r>r_{\mathrm{b}}.\end{cases} \tag{4}$$

Here, the absorbing boundary is $r_{\mathrm{b}}=30$ a.u. and $\beta=1$ a.u. Thus, we can obtain the ionization part of the time-dependent

electronic wave function $[1-g(\boldsymbol{r})]\psi(\boldsymbol{r},t)$, and then a Fourier transformation of $[1-g(\boldsymbol{r})]\psi(\boldsymbol{r},t)$ yields the MF-PMDs.

3. Results and discussion

We first present MF-PMDs of the HOMO and HOMO-1 orbitals for CO_2 aligned along the x-axis exposed to a CP soft x-ray laser pulse. The laser wavelength, intensity and duration are chosen as $\lambda_0 = 5$ nm ($\omega_0 = 9.11$ a.u.), $E_0 = 1.07$ a.u. ($I_0 = 4\times10^{16}$ W/cm^2, and $T_0 = 1000$ as, respectively. From Fig. 2 one finds that the MF-PMDs present twelve-lobe patterns for HOMO and ten-lobe patterns for HOMO-1 in the CP case, and the photoionization distributions are both symmetric about the x-axis for these two orbitals [see Figs. 2(a1) and 2(b1)]. We also present the MF-PMDs for the parallel (parallel to x-axis) and perpendicular (perpendicular to x-axis) linearly polarized fields. For HOMO, there are eight-lobe patterns in both the parallel and perpendicular cases, four-lobe patterns in the parallel case and ten-lobe patterns in the perpendicular case for HOMO-1. In addition, from the results shown in Fig. 2, we can see that the MF-PMDs in the CP case are the sum of those in the parallel and perpendicular linearly polarized cases.

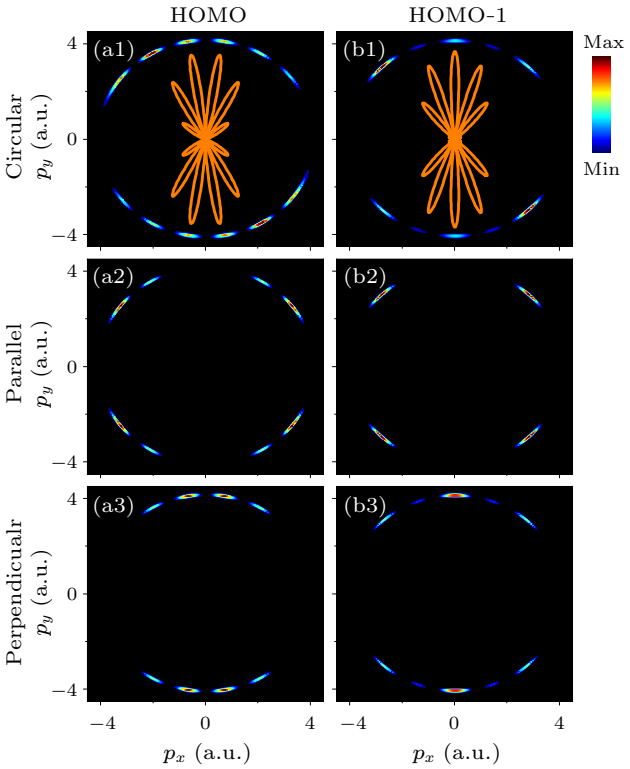


Fig. 2. Molecular-frame photoelectron diffraction patterns for the CO_2 molecule exposed to [(a1), (b1)] CP laser pulses, [(a2), (b2)] parallel and [(a3), (b3)] perpendicular linearly polarized laser pulses. The laser parameters are $\lambda_0 = 5$ nm, $E_0 = 1.07$ a.u., and $T_0 = 60\tau_0$. The prediction of ultrafast photoionization models obtained from Eqs. (7) and (8) is shown in the insets.

These multiple angular nodes of the MF-PMDs reflect the interference dynamics of molecular multi-center photoionization processes. A ultrafast photoionization model based on δ-function pulse is adopted to describe these phenomena, which has been demonstrated to be effective to analyze the ionization process of H_2^+.[16] For the CO_2 molecule, the wavefunction of HOMO is given by $\psi_0(\boldsymbol{r}) = [\psi_{2p_y}(\boldsymbol{r}-\boldsymbol{R}_{L,O}) - \psi_{2p_y}(\boldsymbol{r}-\boldsymbol{R}_{R,O})]/\sqrt{2}$, and that of HOMO-1 is given by $\psi_0'(\boldsymbol{r}) = [\psi_{2p_y}(\boldsymbol{r}-\boldsymbol{R}_{L,O}) + \psi_{2p_y}(\boldsymbol{r}-\boldsymbol{R}_{R,O})]/\sqrt{2}$, a linear combination of the $2p_y$ orbitals which lie on the oxygen atoms at positions $\pm R_{C-O}$. Then, the momentum distribution of photoelectron for HOMO [$\mathcal{F}_{CO_2}(\boldsymbol{p})$] and HOMO-1 [$\mathcal{F}'_{CO_2}(\boldsymbol{p})$] orbitals can be given by

$$\mathcal{F}_{CO_2}(\boldsymbol{p}) \propto |\sqrt{2}(\boldsymbol{n}\cdot\boldsymbol{e})\sin(\boldsymbol{P}\cdot\boldsymbol{R}_{C-O})|^2\psi^2_{2p_y}(|\boldsymbol{p}|), \quad (5)$$

$$\mathcal{F}'_{CO_2}(\boldsymbol{p}) \propto |\sqrt{2}(\boldsymbol{n}\cdot\boldsymbol{e})\cos(\boldsymbol{P}\cdot\boldsymbol{R}_{C-O})|^2\psi^2_{2p_y}(|\boldsymbol{p}|). \quad (6)$$

Here, $\boldsymbol{n}$ and $\boldsymbol{e}$ are the transition dipole vector and the electric field vector, respectively. The terms $\sin(\boldsymbol{P}\cdot\boldsymbol{R})$ and $\cos(\boldsymbol{P}\cdot\boldsymbol{R})$ present the interference effects of the outgoing electron wave packets with same amplitudes emitting from different nuclei. $\boldsymbol{P} = \boldsymbol{p} + \boldsymbol{E}$, $\boldsymbol{p}$ is the photoelectron momentum. $\boldsymbol{E}$ can be ignored in our study, i.e., $\boldsymbol{p} \approx \boldsymbol{P}$ since the ponderomotive energy $U_p \ll I_p$ and $E \ll$ p at intensity $E_0 = 1.07$ a.u. ($I_0 = 4\times10^{16}$ W/cm^2) and $E_1 = 5.34\times10^{-2}$ a.u. ($I_1 = 1\times10^{14}$ W/cm^2). The ultrafast photoionization models in Eqs. (5) and (6) show that one can shift the total photoelectron distributions by momentum of the field $\boldsymbol{E}$ through the δ-function pulse. Moreover, one notes that the wavefunction shape of the ψ_{2p_y} orbital is proportional to the function of $\sin(\theta)$. Then, the MF-PMDs can be written as

$$\mathcal{F}_{CO_2}(\boldsymbol{p}) \sim |\sin(\theta)\sin[pR_{C-O}\cos(\theta)]|^2, \quad (7)$$

$$\mathcal{F}'_{CO_2}(\boldsymbol{p}) \sim |\sin(\theta)\cos[pR_{C-O}\cos(\theta)]|^2, \quad (8)$$

where θ is the angle between the photoelectron momentum $\boldsymbol{p}$ and the molecular $\boldsymbol{R}$ axis, $\mathcal{F}_{CO_2}(\boldsymbol{p})$ is for HOMO, and $\mathcal{F}'_{CO_2}(\boldsymbol{p})$ is for HOMO-1.

From the energy conservation it follows that the corresponding photoelectron momentum is $p = \sqrt{2(\hbar\omega - I_p)} = 4.15$ a.u. and $\lambda_{CO_2} = 2\pi/p = 1.51$ a.u. Since $\lambda_{CO_2} < R_{C-O}$, photoelectron diffraction occurs. The insets in Figs. 2(a1) and 2(b1) present the predicted results of ultrafast photoionization models. For the 5 nm laser pulse at photon energy $\omega_0 = 9.11$ a.u., twelve angular nodes for HOMO and ten angular nodes for HOMO-1 are therefore obtained due to molecular photoelectron diffraction where $\lambda_{CO_2} < R_{C-O}$. One can see that the theoretical prediction of angular nodels obtained from Eqs. (7) and (8) and the results of TDSE simulations are coincident, confirming that the ultrafast photoionization models can well describe photoelectron diffraction process and the validity of the SAE model in ultrafast molecular high-frequency photoionization.

Figure 2 presents the results by a soft x-ray pulse, thus giving rise to photoelectron diffraction. The photon and photoelectron energies are much larger than the ionization energy,

that is, $\omega \gg I_p$. The molecular Coulomb effects are negligible in photoionization. Therefore, MF-PMDs are determined by both the molecular orbital symmetry and the photoelectron momentum $\boldsymbol{p}$. However, for the process with the photon energy slightly larger than the ionization energy, $\omega > I_p$, the photoelectrons have lower kinetic energies, where the Coulomb effect has strongly influences on the molecular photoionization. We next consider the molecular photoionization process by an XUV pulse with a longer wavelength.

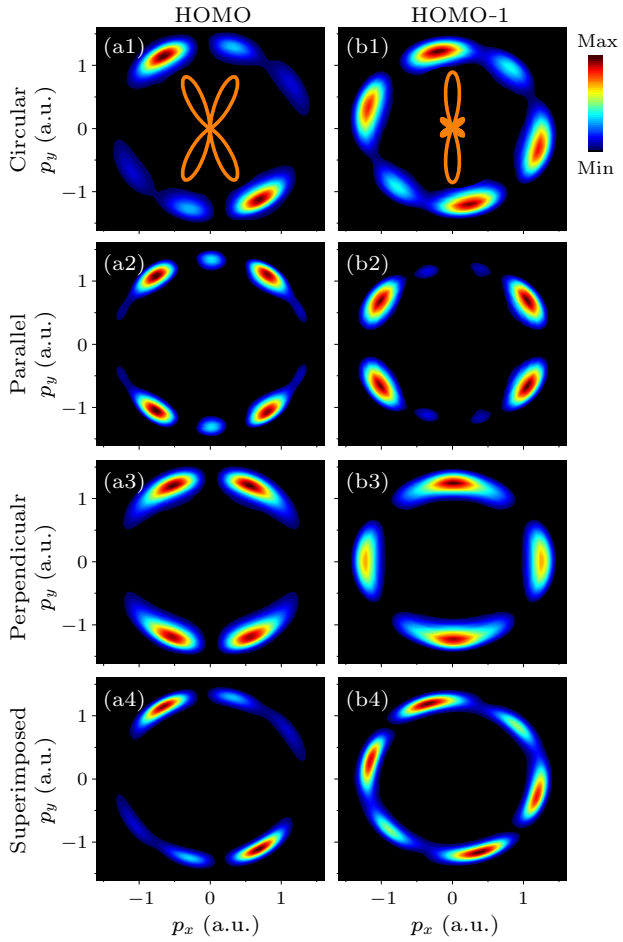


Fig. 3. The MF-PMDs for the CO_2 molecule exposed to the driving laser pulses with $\lambda_1 = 30$ nm, $E_1 = 5.34 \times 10^{-2}$ a.u., and $T_1 = 10\tau_1$. Labels (1)–(3) present the MF-PMDs in CP fields, parallel and perpendicular linearly polarized laser fields; (a) and (b) present HOMO and HOMO-1 orbitals, respectively. (a4)–(b4) Superpositions of MF-PMDs in the parallel and perpendicular cases. The prediction of ultrafast photoionization models obtained from Eqs. (7) and (8) is shown in the insets.

Different from the MF-PMDs in Fig. 2, the results of CO_2 molecules exposed to a CP laser pulse with wavelength $\lambda_1 = 30$ nm ($\omega_1 = 1.52$ a.u.) are shown in Fig. 3. The change of the MF-PMDs with different wavelengths reflects the dependence of the MF-PMDs on the photoelectron momentum p. Therefore, varying the pulse wavelength gives rise to different structures of the MF-PMDs. Single-photon ionization process occurs since $\omega > I_p$. The corresponding momentum and de Broglie wavelength are $p' = 1.42$ a.u. and $\lambda'_{CO_2} = 4.42$ a.u., respectively. Apparently, no diffraction occurs due to $\lambda'_{CO_2} > R_{C-O}$. The angles of the photoelectron distributions are localized at 34°, 77°, 121°, 214°, 257°, and 304° for the HOMO orbital [see Fig. 3(a1)], and 49°, 99°, 164°, 229°, 283°, and 344° for the HOMO-1 case [see Fig. 3(b1)]. In the insets of Figs. 3(a1) and 3(b1), we also plot the theoretically predicted results obtained from the ultrafast photoionization models. However, for the MF-PMD of CO_2 molecule with 30 nm, there is a deviation between the angle nodes predicted by the ultrafast photoionization models and those of the MF-PMDs calculated by TDSE, and the angle nodes of the MF-PMDs are generally deflected to the right by a small angle relative to the theoretically predicted results. Meanwhile, the MF-PMDs rotates in the same direction as the helicity of driving laser pulses.[12] Here, the MF-PMDs are rotated to the right because the right-handed laser pulse is used [see Figs. 3(a1) and 3(b1)].

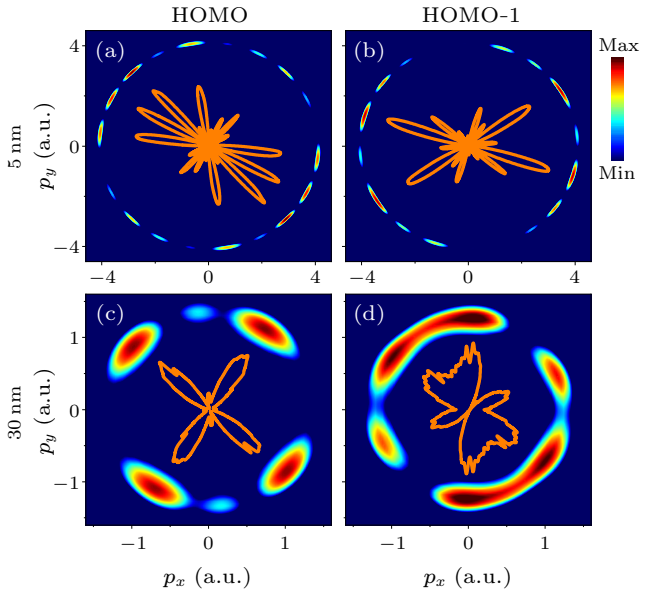


Fig. 4. Coherent sum of MF-PMDs for the CO_2 molecule at different molecular alignment angles (0°, 18°, 36°, 54°, 72°, 90°, 108°, 126°, 144°, 162°, 180°, 198°, 216°, 234°, 252°, 270°, 288°, 306°, 324°, and 342°) exposed to a CP laser pulse. The laser wavelengths are 5 nm for (a) and (b) and 30 nm for (c) and (d). The other laser parameters are same as those used in Figs. 2 and 3.

To further interpret the helicity of the MF-PMDs, we numerically calculate the MF-PMDs exposed to linearly polarized laser pulses with wavelength $\lambda_1 = 30$ nm [see Figs. 3(a2), 3(b2) (parallel) and 3(a3), 3(b3) (perpendicular)]. The laser wavelength, intensity and duration are the same as those in Fig. 3(a1). MF-PMDs for the HOMO by a parallel linearly polarized laser pulse have six components with the momentum $p' = 1.42$ a.u. localized at 56°, 90°, 124°, 236°, 270°, and 308°, as shown in Fig. 3(a2). For the perpendicular case in Fig. 3(a3), the four angles of the MF-PMDs are localized at 67°, 113°, 247°, and 293°. Compared with the angle of MF-PMDs in the CP case [see Fig. 3(a1)], the angles of the sum for those in the parallel and perpendicular cases are somewhat deflected. Accordingly, the CP laser pulse can

be decomposed into two perpendicular linearly polarized laser pulses, and such a decomposition rule is also applied to H_2^+ molecules.[19] Therefore, we add up coherently the wavefunctions of final states in coordinate space for the parallel and perpendicular linearly polarized fields, and transform the superimposed wavefunction to the momentum space. The superposition of both parallel and perpendicular ionizations for HOMO in Fig. 3(a4) is in good agreement with the MF-PMDs in Fig. 3(a1). Similarly, this superposition for the HOMO-1 is also valid [see Figs. 3(b1) and 3(b4)]. Thus, the results of the CO_2 molecule for CP ionization can be viewed as the superposition of both parallel and perpendicular linearly polarized ionizations.

If the molecules are not perfectly aligned in the experiment, the laboratory-frame photoelectron momentum distributions (LF-PMDs) can be given by coherent summations of MF-PMDs weighted by the molecular axis alignment moments. The superposition of the MF-PMDs at different orientation angles may lead to a vanishing or weakening of the anisotropic angular distribution. For example, in Fig. 4 we present the MF-PMDs for the CO_2 molecules with equal weighted at different alignment angles. For simplicity, we assume $\boldsymbol{P}_0 = 0$. As is expected, the peaks of the weighted MF-PMDs are different from the original ones [Figs. 2(a1), 2(b1) and 3(a1), 3(b1)]. We can get the conclusion that different orientation angles lead to a gradually vanishing of the anisotropic angular distribution.

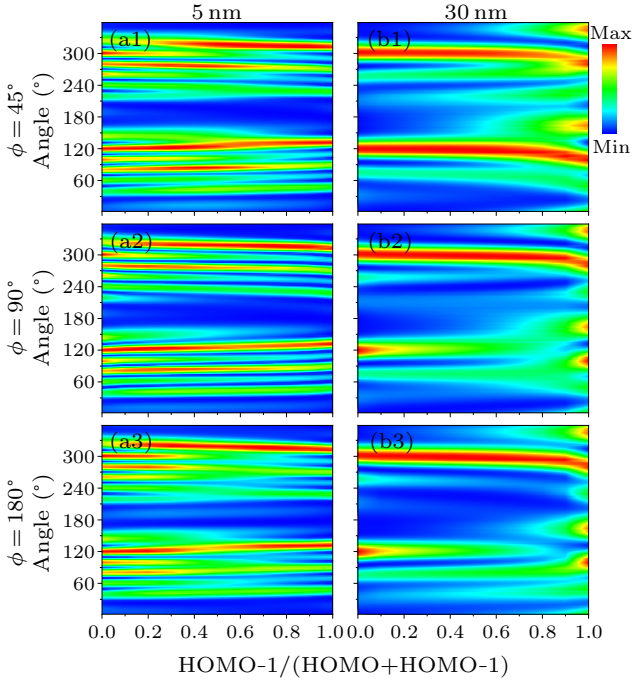


Fig. 5. Ionization yields as functions of relative phase and the ratio of HOMO-1 and HOMO orbitals for different alignment angles exposed to a CP laser pulse.

We also study the contribution of different ratios of HOMO and HOMO-1 orbitals to photoionization. Figure 5 presents the ionization yields as functions of relative phase and the ratio of HOMO and HOMO-1 for different orientation angles. We can see that for 5 nm, the ionization yield is always maximum at about 120° and 320° for different ratios of these two orbitals, and is also independent of the relative phase [see Figs. 5(a1)–5(a3)]. However, the ionization yields present different tendencies for 30 nm. When the relative phase is 45°, the ionization yields are always maximum at about 120° and 300° as the ratio changes from 0 to 1, and the two branches show monotonically decreasing, as illustrated in Fig. 5(b1). As the relative phase increases to 90° and 180°, the ionization yield with an angle of 120° decreases with the increasing ratio [see Figs. 5(b2) and 5(b3)]. Our results demonstrate that we can determine the contribution of HOMO and HOMO-1 orbitals to ionization by varying the relative phase and the ratio of the HOMO and HOMO-1.

4. Conclusions

In summary, we have theoretically studied ultrafast MF-PMDs for imaging molecular orbital structures by means of numerically solving the TDSE within frozen-nuclei and SAE frames. The photoionization processes from the HOMO and HOMO-1 orbitals of the CO_2 molecule are presented by CP attosecond laser pulses. It is found that for a soft x-ray laser pulse with wavelength 5 nm, photoelectron diffraction patterns are produced, which can be exactly described by the ultrafast photoionization models. With wavelength of 5 nm, the photoelectron energy is much larger than the molecular ionization energy and the Coulomb effect is negligible. For comparison, we present the process by an XUV pulse with 30 nm. In lower XUV energy photoelectron processes, a distortion of the MF-PMDs occurs, and the angle nodes of the MF-PMDs are generally deflected to the right by a small angle relative to the theoretically predicted results of the ultrafast photoionization models. Our results demonstrate that the MF-PMDs of the CO_2 molecule in a CP field are the superposition of both parallel and perpendicular linearly polarized fields. In addition, the ionization yields as functions of relative phase and the ratio of HOMO and HOMO-1 orbitals for different alignment angles are investigated and we present a scheme to determine the contribution of HOMO and HOMO-1 orbitals to ionization, which offers the possibility for imaging ultrafast intramolecular dynamics with attosecond resolutions by using the MF-PMDs.

Acknowledgments

Project supported by the National Natural Science Foundation of China (Grant Nos. 11974007, 12074146, 12074142, 61575077, 12374265, 11947243, 91850114, and 11774131) and the Natural Science Foundation of Jilin Province of China (Grant No. 20220101016JC).

References

[1] Brabec T and Krausz F 2000 *Rev. Mod. Phys.* **72** 545
[2] Messina F, Bräm O, Cannizzo A and Chergui M 2013 *Nat. Commun.* **4** 2119
[3] Wang L, Wang X, Xiao F, Wang J, Tao W, Zhang D and Zhao Z 2023 *Chin. Phys. Lett.* **40** 113201
[4] Zhao J, Liu J, Wang X, Yuan J and Zhao Z 2022 *Chin. Phys. Lett.* **39** 123201
[5] Tanaka H, Yabashi M, Asaka T, *et al.* 2012 *Nat. Photon.* **6** 540
[6] Xu J, Blaga C I, Agostini P and DiMauro L F 2016 *J. Phys. B: At. Mol. Opt. Phys.* **49** 112001
[7] Nan Q W, Wang C, Yu X Y, Zhao X, Cheng Y, Gong M, Liu X J, Kimberg V and Zhang S B 2023 *Chin. Phys. Lett.* **40** 093201
[8] Küpper J, Stern S, Holmegaard L, *et al.* 2014 *Phys. Rev. Lett.* **112** 083002
[9] Jiang Y H, Rudenko A, Plésiat E, *et al.* 2010 *Phys. Rev. A* **81** 021401
[10] Underwood J G and Reid K L 2000 *J. Chem. Phys.* **113** 1067
[11] Pullen M G, Wolter B, Le A T, *et al.* 2015 *Nat. Commun.* **6** 7262
[12] Odenweller M, Takemoto N, Vredenborg A, *et al.* 2011 *Phys. Rev. Lett.* **107** 143004
[13] Lei Z X, Xu Q Y, Yang Z J, He Y L and Guo J 2022 *Chin. Phys. B* **31** 063202
[14] Yang H, Liu X, Zhu F, Jiao L and Liu A 2024 *Chin. Phys. B* **33** 013303
[15] Mauritsson J, Remetter T, Swoboda M, *et al.* 2010 *Phys. Rev. Lett.* **105** 053001
[16] Zuo T, Bandrauk A D and Corkum P B 1996 *Chem. Phys. Lett.* **259** 313
[17] Meckel M, Comtois D, Zeidler D, *et al.* 2008 *Science* **320** 1478
[18] Peters M, Nguyen-Dang T T, Charron E, Keller A and Atabek O 2012 *Phys. Rev. A* **85** 053417
[19] Yuan K J, Lu H and Bandrauk A D 2011 *Phys. Rev. A* **83** 043418
[20] Dou Y, Fang Y, Ge P and Liu Y 2023 *Chin. Phys. Lett.* **40** 033201
[21] Geng L, Liang H and Peng L Y 2022 *Chin. Phys. Lett.* **39** 044203
[22] Peters M, Nguyen-Dang T T, Cornaggia C, Saugout S, Charron E, Keller A and Atabek O 2011 *Phys. Rev. A* **83** 051403
[23] Pengel D, Kerbstadt S, Johannmeyer D, Englert L, Bayer T and Wollenhaupt M 2017 *Phys. Rev. Lett.* **118** 053003
[24] Pengel D, Kerbstadt S, Englert L, Bayer T and Wollenhaupt M 2017 *Phys. Rev. A* **96** 043426
[25] Ma M Y, Wang J P, Jing W Q, Guan Z, Jiao Z H, Wang G L, Chen J H and Zhao S F 2021 *Opt. Express* **29** 33245
[26] Djiokap J M N, Meremianin A V, Manakov N L, Hu S X, Madsen L B and Starace A F 2017 *Phys. Rev. A* **96** 013405
[27] Skruszewicz S, Tiggesbäumker J, Meiwes-Broer K H, Arbeiter M, Fennel T and Bauer D 2015 *Phys. Rev. Lett.* **115** 043001
[28] Lein M, Hay N, Velotta R, Marangos J P and Knight P L 2002 *Phys. Rev. Lett.* **88** 183903
[29] van der Zwan E V and Lein M 2010 *Phys. Rev. A* **82** 033405
[30] Lai X and Figueira de Morisson Faria C 2013 *Phys. Rev. A* **88** 013406
[31] Hu S, Chen J, Hao X and Li W 2016 *Phys. Rev. A* **93** 023424
[32] Ilchen M, Glaser L, Scholz F, *et al.* 2014 *Phys. Rev. Lett.* **112** 023001
[33] Ansari Z, Böttcher M, Manschwetus B, *et al.* 2008 *New J. Phys.* **10** 093027
[34] Kunitski M, Eicke N, Huber P, *et al.* 2019 *Nat. Commun.* **10** 1
[35] Okunishi M, Itaya R, Shimada K, *et al.* 2009 *Phys. Rev. Lett.* **103** 043001
[36] Busuladžić M, Gazibegović-Busuladžić A, Milošević D B and Becker W 2008 *Phys. Rev. Lett.* **100** 203003
[37] Hässig M, Altwegg K, Balsiger H, *et al.* 2015 *Science* **347** aaa0276
[38] Zhu X, Liu X, Li Y, Qin M, Zhang Q, Lan P and Lu P 2015 *Phys. Rev. A* **91** 043418
[39] Hu S L, Zhao Z X and Shi T Y 2013 *Chin. Phys. Lett.* **30** 103103
[40] Li Y, Qin M, Zhu X, Zhang Q, Lan P and Lu P 2015 *Opt. Express* **23** 10687
[41] https://webbook.nist.gov/chemistry/
[42] Feit M D, Fleck J A and Steiger A 1982 *J. Comput. Phys.* **47** 412